Seaglider: A Long-Range Autonomous Underwater Vehicle for Oceanographic Research

Charles C. Eriksen, T. James Osse, Russell D. Light, Timothy Wen, Thomas W. Lehman, Peter L. Sabin,
John W. Ballard, and Andrew M. Chiodi

Abstract—Seagliders are small, reusable autonomous underwater vehicles designed to glide from the ocean surface to a programmed depth and back while measuring temperature, salinity, depth-averaged current, and other quantities along a sawtooth trajectory through the water. Their low hydrodynamic drag and wide pitch control range allows glide slopes in the range 0.2 to 3. They are designed for missions in range of several thousand kilometers and durations of many months. Seagliders are commanded remotely and report their measurements in near real time via wireless telemetry. The development and operation of Seagliders and the results of field trials in Puget Sound are reported.

Index Terms—Marine vehicles, mobile robots, sea measurements, underwater vehicles.

I. INTRODUCTION

SMALL, smart, inexpensive instrument platforms offer the promise of describing the ocean interior with much higher resolution in space and time than is possible with techniques reliant on ships and moorings. Autonomous floats [1] have demonstrated the power of a distributed network to describe circulation at comparatively modest cost [2]. Profiling versions of these floats are poised to monitor the large-scale hydrographic structure of the ocean interior [3]. Stommel [4] fantasized a global network of inexpensive glider vehicles powered by thermal energy extracted from the ocean thermocline that could be directed to sample specific transects. Here we describe a battery-powered autonomous underwater vehicle (AUV) we call Seaglider designed to profile up to about 1500 km of the ocean vertically and 6000 km horizontally under remote control over many months.

Historically, the density in space and time of oceanographic observations has been limited by the cost of operating ships. Ship surveys tend to last no more than a month or two and, with rare exceptions (e.g., the Hawaii-Tahiti Shuttle Experiment [5]), are not repeated often enough and over a sufficiently long duration to resolve dominant space–time variability in the ocean. Moorings offer a superior technique to a stationary ship for resolving temporal variability, but again, with rare exceptions (e.g., the TOGA-TAO array [6]), moored arrays are too sparse and short-lived to resolve the dominant space–time variability of oceanic flows. Moorings, of course, rely on ships for deployment and recovery and are anchored at fixed locations chosen in advance. Stommel [7] remarked that determination of atmospheric climatology by means analogous to those used by oceanographers would be to use "half a dozen automobiles and kites to which air sounding instruments were attached and by doing all of their work on dark moonless nights when they couldn't see what was happening in their medium." While ocean instrumentation has progressed greatly in the last half century, until the last few years, oceanographers have been largely limited by cost to relatively few platforms from which to examine the ocean interior.

We view the development of an autonomous glider as a means of greatly extending the density of hydrographic observations at orders of magnitude lower cost than is possible with ships and moorings. The construction cost of a glider is equivalent to a few days of ship time and its annual operational cost is equivalent to a fraction of a ship day. Seagliders are reusable (nonpolluting), can be deployed from small boats, are controlled remotely, and report their measurements shortly after they are made. They can be used on the same mission to alternately travel along a commanded path in the manner of a ship survey or maintain their geographic position by profiling vertically against ambient currents, sampling virtually as a mooring does. Our vehicle was originally conceived as a "Virtual Mooring Glider," but is now called Seaglider because the name is more descriptive of its operation.

Section II describes the hydrodynamic, mechanical, electrical, and software design of the Seaglider. Section III describes its performance in field trials in Puget Sound. The paper concludes with a brief discussion of potential uses of Seagliders.

II. VEHICLE DESCRIPTION

A. Component and Operation Summary

The Seaglider consists of a pressure hull enclosed by a fiberglass fairing to which wings, rudders, and a trailing antenna are attached (Fig. 1). Energy use, cost, reliability, and ease of operation guided the design. To achieve vehicle ranges comparable to ocean basin dimensions, an energy-efficient design was essential. We chose a low-drag vehicle shape combined with a pressure hull that is nearly neutrally compressible in seawater, the combination of which led to the fairing-hull configu-

Fig. 1. Top view of three Seaglider vehicles in their handling cradles on deck. Plastic tubing is connected to the conductivity cell mounted atop the pink fairing just aft of its maximum diameter between the wings on two of the three vehicles. The white antenna masts extend aft of the fairings outside the view of this image.

ration. Propulsion is provided by buoyancy control effected by variation of vehicle-displaced volume. Wings provide hydrodynamic lift to propel the vehicle forward as it sinks or rises. In contrast to propeller-driven AUVs whose mission durations and ranges are measured in hours and tens of kilometers, a buoyancy-driven vehicle can achieve mission durations of over a year and ranges comparable to ocean basin widths simply by traveling slowly. Because drag scales roughly as the square of vehicle speed, halving speed quadruples mission duration and doubles vehicle range. In contrast to aerodynamic gliders (sailplanes), Seagliders glide both as they dive and as they climb by adjusting their volume to be either slightly smaller or larger than that of an equal mass of seawater. Attitude control is accomplished by moving mass within the vehicle, obviating the need for active external control surfaces and their inherent complexity.

To keep the cost modest and allow it to be launched and recovered from small boats, vehicle size was chosen to be just big enough to carry the constituent parts, namely a buoyancy control system centered on a small high-pressure pump and the batteries and electronics to run the vehicle. The Seaglider fairing is 1.8 m long, its wings span 1 m, and the antenna mast is 1.4 m long. The vehicles weigh 52 kg so they are easily carried by two people.

Seaglider alternately dives and climbs to a commanded depth, executing a sawtooth path through the ocean. At the sea surface, the vehicle pitches downward by about 45° to expose its antennas, one to receive Global Positioning System (GPS) fixes and the other to transmit measurement data and receive commands. Based on its distance to a target position, the vehicle chooses a glide slope and bearing to approach the target. By choosing a speed and direction in opposition to current averaged over its dive depth, it can profile vertically at a fixed geographic position (the "virtual mooring" mode). Seaglider uses the difference between its dead-reckoned and actual displacements to estimate depth-averaged current.

B. Hydrodynamic Design

1) Low Drag Shape: Efficient hydrodynamic design is essential to glider performance. A buoyancy-powered AUV expends energy against hydrodynamic drag, differential compressibility between the vehicle and seawater, and ocean stratification. Even at the relatively slow speeds envisioned for Seaglider, drag is the largest of these expenditures, contributed mainly by skin friction. Our approach was to adopt a proven low-drag shape and add wings to it. We adopted the low-drag shape [8] used to develop a small mobile target vehicle (AEMT[9]) able to maintain laminar flow over more than 80% of its surface area at speeds as high as 7 m/s. This axisymmetric shape employs a comparatively long, gently tapered foresection that acts to maintain laminar boundary layer flow while the aftersection, where boundary flow is turbulent, makes up a small fraction of the overall wetted surface.

Seagliders were designed to operate over a range of glide slopes so that they could efficiently both maintain geographic position while profiling and make vertical sections along survey transects as desired. Steep trajectories are most efficient for a virtual mooring mission, while relatively gentle ones are better for a survey. Glide slopes steeper than ocean water property slopes are necessary to resolve oceanic structure, so that glide slopes gentler than about 1 : 5 are unnecessary. Vehicle speeds have to equal or exceed that of currents averaged over the vertical extent of dives in order for gliders to maintain position or make deliberate ground speed against current, but range is extended by traveling more slowly through the water. A vehicle designed to travel about 0.25 m/s satisfies the needs for ocean basin scale range, the ability to counter modest ocean currents, and resolve space–time structure of low-frequency oceanic variability.

Steady flight dynamics describe glider motion where control states are maintained for sufficiently long periods of time. For glider translation along a direction inclined at glide angle θ from horizontal, vehicle lift L and drag D are balanced by projections of the buoyancy force B (positive upwards)

$$L = ql^2 a\alpha = -B\cos\theta \qquad (1)$$
$$D = ql^2(bq^{-(1/4)} + c\alpha^2) = B\sin\theta \qquad (2)$$

where dynamic pressure $q = \rho/2(U^2 + W^2)$ is defined by water density ρ and horizontal and vertical speed components U and W and l is the hull length. It is assumed that lift is proportional to the attack angle α and drag is comprised of profile and induced drag components. It has been shown from boundary layer considerations that hull drag for the chosen shape [9] is proportional to (speed)$^{3/2}$, giving the parameterization of the profile drag coefficient as $bq^{-(1/4)}$. The drag induced by lift is parameterized as proportional to the square of the attack angle. The vehicle pitch angle ϕ is related to the attack and glide angles by $\phi = \theta + \alpha$. The glide slope is given by the ratio of drag to lift, $\tan\theta = W/U = -D/L$, and buoyancy is the vector sum of lift and drag $B^2 = D + L^2$. Note that the attack angle α has the opposite sign from the glide and pitch angles θ and ϕ, so that the glide angle exceeds pitch angle in magnitude.

From the substitution of (1) into (2), an expression for vertical speed W in terms of horizontal speed U can be written as

$$W = \frac{bl^2}{B}\left(\frac{\rho}{2}\right)^{1-(\gamma/2)}\frac{U^{3-\gamma}}{\cos^{3-\gamma}\theta} + \frac{2cB}{a^2 l^2 \rho}\frac{\cos^3\theta}{U} \quad (3)$$

where the parameter γ takes the value 0.5 for the Seaglider hull shape. This equation, in the limit of small glide angle (i.e., nearly horizontal flight so $\cos^3\theta \approx 1$), is identical to that used commonly in aerodynamic literature to describe the so-called "glide polar" for a sailplane [10, eq. (6a)]. For the steeper glide angles appropriate to Seaglider performance, the gentle glide slope approximation is violated and (3) is more conveniently expressed as a quadratic equation in buoyancy B or nearly quadratic in dynamic pressure q

$$(ql^2)^2 bq^{-(1/4)} - Bql^2\sin\theta + B^2 ca^{-2}\cos^2\theta = 0. \quad (4)$$

Eliminating buoyancy from (1) and (2) gives an expression quadratic in attack angle α

$$c\alpha^2 + a\alpha\tan\theta + bq^{-(1/4)} = 0. \quad (5)$$

Solutions to (4) for buoyancy and dynamic pressure and to (5) for attack angle are

$$B = \frac{ql^2 a^2 \sin\theta}{2c\cos^2\theta}\left(1 \pm \sqrt{1 - \frac{4}{\Lambda\tan^2\theta}}\right) \quad (6)$$

$$q = \frac{B\sin\theta}{2l^2 bq^{-(1/4)}}\left(1 \pm \sqrt{1 - \frac{4}{\Lambda\tan^2\theta}}\right) \quad (7)$$

$$\alpha = \frac{-\alpha}{2c}\tan\theta\left(1 \pm \sqrt{1 - \frac{4}{\Lambda\tan^2\theta}}\right) \quad (8)$$

where the performance factor Λ is defined by the ratio of the lift coefficient squared to the product of drag coefficient and induced drag coefficient: $\Lambda = a^2/bq^{-(1/4)}c$. The upper sign in each expression corresponds to glides where profile drag exceeds induced drag. These are preferred since they give higher speed and lower attack angle for a given buoyancy. The minimum glide slope is $2/\sqrt{\Lambda}$ and occurs when profile and induced drag are equal [the discriminant in (6)–(8) vanishes]. Smaller drag coefficients (higher performance factors) permit gentler glide slopes, hence more horizontal range for a given depth excursion.

The lift, profile drag, and induced drag coefficients a, b, and c determine vehicle performance. These are not known *a priori* and must be determined experimentally. Estimates of these parameters have been obtained in three ways: in wind tunnel tests on a scaled version of Seaglider, by tracking a glider in a fjord while simultaneously observing currents, and by comparing model to observed vertical velocity of gliders over hundreds of dive cycles in a fjord. Results of the field determinations of glider performance are discussed below in Section III.

The hydrodynamic design of Seaglider was carried out by R. M. Hubbard (Hubbard Engineering, Lopez Island, WA). In addition to scaling the AEMT vehicle shape and choosing wing and rudder sizes and placements, Hubbard helped design and carry out a series of wind tunnel tests on the AEMT hull (0.92 m long) appended with wings and rudder fins. These tests were carried out in the Low-Speed Wind Tunnel of the University of Washington (UW) Aerodynamics Laboratory, a tunnel with an approximately 1-m-square test section. The modified AEMT hull was mounted from aft on a shaft along the hull centerline with a small three-axis force/torque sensor (Assurance Technologies, Inc., model F/T Nano) capable of detecting the $O(1–10\text{ g})$ lift and drag forces induced by wind.

Flow visualization studies were carried out in the wind tunnel by observing drying patterns of a kerosene–talcum powder mixture for different wind speeds and attack angles. The technique demonstrated that laminar flow separates just aft of the maximum diameter of the body and reattaches turbulently near the tail for attack angles as high as $12°$.

The wind tunnel measurements could not simulate hydrodynamic forces induced by the trailing antenna mast nor of the conductivity–temperature sensor sail, but they did give an indication of how important seemingly small appendages are to glide performance. While an appended toroidal model conductivity sensor had only about 2% of the frontal cross-sectional area of the AEMT, it accounted for more than 25% of the total drag. Partly in an attempt to reduce drag, an electrode conductivity sensor from Sea-Bird Electronics was selected for Seaglider. Its cross-sectional area, including a faired mount, is less than half that of the toroidal sensor considered in the wind tunnel.

Wings and Rudders: In addition to the goal of determining vehicle drag in the UW Low Speed Wind Tunnel, we wanted to confirm that use of wings on a low-drag vehicle would not adversely affect its flow characteristics. Fears of increased turbulent flow, disrupted forebody laminar flow, turbulent separation on the aftersection or instability in the flow regime over a control region were allayed by results of the wind tunnel studies. Wings had to be located aft of the maximum body diameter where the two part fairing mates.

Wing span was arbitrarily limited to 1 m in order to facilitate handling at sea and assure strength when fabricated of syntactic foam. High-aspect-ratio wings were unnecessary for the modest glide slopes called for by ocean sampling strategy. We chose the NACA 16-006 airfoil section for both the main wings and rudder sections. This profile was shown to exhibit low drag primarily due to the formation of a laminar separation bubble that formed at the leading edge, followed by laminar flow through to about 80% of the chord, even at moderately high angles of attack. This laminar flow separation bubble had the effect of increasing the leading edge radius, more like that found on the more common NACA 009 section, but benefited from the favorable pressure regime downstream of the reattached bubble, unlike that which exists on the thicker NACA 009 airfoil section. This was confirmed with the previously mentioned flow visualization studies. Earlier studies in support of AEMT development showed this airfoil section to provide the highest overall lift to drag ratio for low Reynolds number AUVs.

C. Mechanical Design

Layout: The vehicle shape is provided by a fiberglass fairing which encloses the pressure hull (Fig. 2). The low-drag fairing
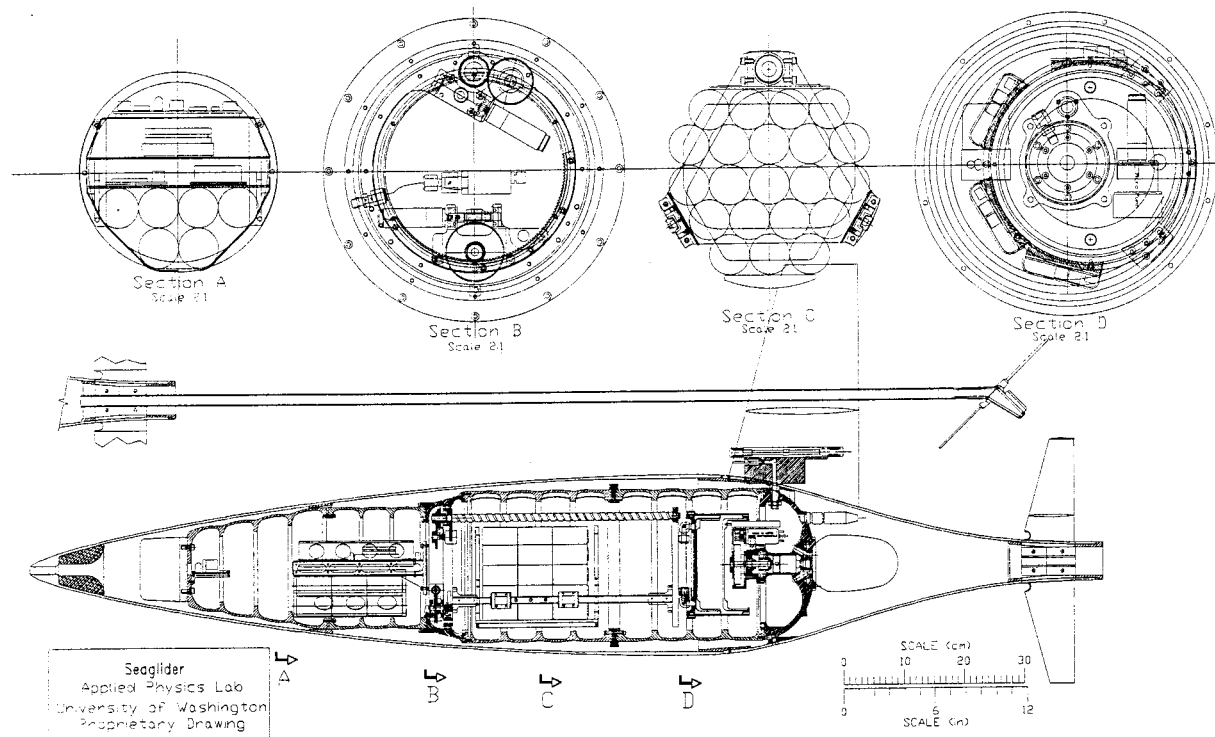
Fig. 2. Schematic design of Seaglider. The bottom shows a side view with the wing shape provided above for reference. The antenna mast is shown separately above the fairing and pressure hull. Four cross-sectional views at an expanded scale are shown at the top of the figure.

was fabricated from a match mold with a 0.38-cm wall thickness. Pacific Research, Inc., used their filament braiding machine to custom wind a fiberglass sock, braided around our male mold, that was then injected with polyester resin. The results were seamless foresection and aftersection fiberglass sections of high strength and stiffness. Three aluminum rings are inserted at the time of fabrication into cavities on the male mold: one at the junction of the two fiberglass sections, a second at the one and only point where the pressure hull is attached to the fairing, and finally one at the tail, where the rudder and antenna are hard mounted. A small hole is at the nose, allowing limited flushing of the interstitial water volume, and a larger vent at the tail.

The pressure hull is composed of seven different sections. The forward two are permanently joined, as are three sections that comprise the main hull so that the hull breaks into four sections. Different hull sections accommodate the low-drag fairing shape while still being fabricated from commercially available aluminum tubing, with one exception. All hull sections are AA6061-T6 aluminum, adequate to withstand pressures to 1000 dbar.

An acoustic transducer used to locate and track the vehicle is located at the front of the forwardmost hull section. This transducer was used with a custom synchronous tracking range to track Seaglider during hydrodynamic field tests and later replaced by a Datasonics transponder based tracking system. Immediately aft is the Precision Navigation TCM2-80 attitude sensor.

Further aft is the electronics section (Section A of Fig. 2). Here, the custom electronic circuit board of about 325 cm^2, a cellular phone modem, a GPS, and sensor electronics are mounted on a cantilevered bracket. Beneath these is the low-voltage battery pack.

The attitude control system is located aft of the electronics section. Complete vehicle flight control is accomplished by controlling the vehicle center of gravity relative to its center of buoyancy. Center of gravity is additionally changed by changes in vehicle displacement, which also changes its center of buoyancy. This section (Section B of Fig. 2) contains mechanisms to move the high-voltage battery pack fore and aft to control pitch (thus glide slope) and roll it left or right to control vehicle roll (thus turn rate). Both pitch and roll actuations are powered by 16-mm Maxon neodymium magnet motors, driving a four-stage planetary gearbox followed by worm drive and spur gear mechanisms. For the pitch control device, the final gear reduction is a ball screw linear actuator. The worm drive mechanism, present in both, provides not only gear reduction, but the needed brake mechanism. Both mechanisms utilize a multiturn rotary potentiometer driven through a spur gear for closed-loop feedback control to the microprocessor.

The variable buoyancy device (VBD) is located at the aft end of the pressure hull and includes an internal piston reservoir, a pumping system, and an external hydraulic accumulator. The antenna mast is mounted to the narrow tail of the fairing.

Buoyancy Control System: The VBD followed design elements used in ALACE vehicles [1]. Undesirably large weight and volume requirements of other types of mechanical pistons that could provide the desired volume and pressure capability led to the more complicated scheme of hydraulically pumping a fluid from an internal reservoir to an external reservoir. As shown in Section D of Fig. 2, the entire hydraulic mechanism is contained within the aft endcap. A Bellowfram
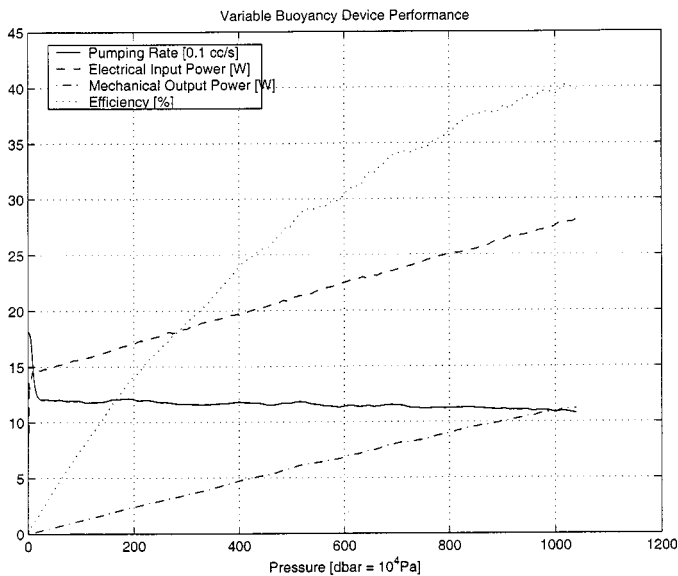
Fig. 3. Buoyancy control system pumping rate, electrical input power (current times voltage), mechanical output power (pressure times rate of volume change), and efficiency (ratio of output to input power) versus pressure.
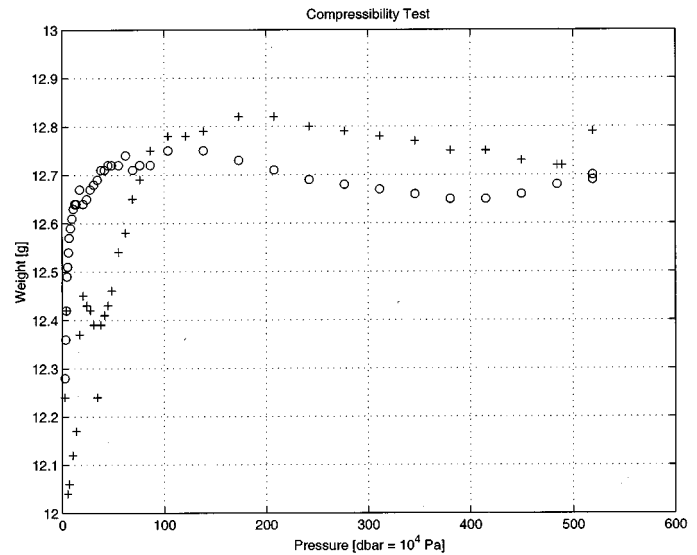

Fig. 4. Weight of Seaglider in a pressure vessel filled with de-ionized fresh water at room temperature. Symbols indicate duplicate tests. Weight changes of $\sim$12 g at pressures lower than 2 dbar due to air bubble compression are not shown in order that resolution at higher pressures may be higher. Differences between the tests can be attributed to load measurement errors.

rolling diaphragm provides an internal hydraulic reservoir. The constant area reservoir allows precise measurement of oil reservoir volume, hence vehicle displacement, by using two linear potentiometers.

Standard very low viscosity hydraulic oil is fed into a boost pump (Micropump model 1601) before being sent to the high-pressure hydraulic axial piston pump (Hydro Rene LeDuc model PB32.5). Early failures were traced to insufficient supply pressure to the piston pump. The addition of a separate boost pump provides the needed supply pressure to the high-pressure pump. (Axial piston pumps are noted for their poor suction abilities.) Oil reenters the internal reservoir via a strategy adapted from ALACE floats. A partial vacuum is drawn on the pressure hull interior so that oil will bleed out of the external hydraulic accumulator under atmospheric pressure. A magnetically latching solenoid valve is used to control the quantity of oil transferred. The internal vacuum exacerbates the main pump oil supply problem, as do variations in vehicle pitch that can place the reservoir below the pump, making the boost pump necessary. With the addition of the boost pump, we have had no problems in several hundred field dives and many thousands of bench runs, most under full load conditions.

VBD performance is shown in Fig. 3 from data collected while the pumping system operated in a closed volume pressure chamber. Axial piston pumps are most efficient at high pressures. To augment the pump rate at near atmospheric pressure, a combination of balanced check valves is used to increase the pumping rate by about 50% with no increase in power consumption. The VBD system consumes $\sim$10 W at atmospheric pressure and close to 15 W at pressures of a few dbar, while at higher pressures the dependence is nearly linear. Power consumption at 1000 dbar is less than twice that at 100 dbar, indicating that the glider is several times more efficient making 1-km-deep dives than dives to typical continental shelf depths.

Isopycnal Hull: Seaglider employs passive compensation for volume changes due to pressure. Volume changes due

to the compressibility difference between a pressure hull and seawater are potentially significant sources of buoyancy. Otherwise uncompensated, they require additional energy expenditure in a buoyancy-powered AUV. While use of a compressee together with a conventional hull can accomplish neutral compressibility, we have taken the approach of designing a hull that is nearly neutrally compressible. This has the advantage of requiring a lighter hull, thus increased internal volume and weight capacity for instrumentation and batteries. The Seaglider hull consists of a series of arched panels supported by ring stiffeners with generous fillets. The goal was to achieve uniformly high hull deflection throughout while maximizing design pressure.

Fig. 4 shows compressibility of the full Seaglider pressure hull, wings, and fairing. These data were obtained using a 500-dbar pressure vessel fitted with a strain-gauge load measurement system designed for water immersion at pressure. The observed changes in weight by less than 0.5 g over more than 500 dbar change in pressure indicate that Seaglider compressibility is within 0.5% of that of the de-ionized room-temperature fresh water used in the test. That is, pressure-induced Seaglider buoyancy changes are negligibly small. This feature extends vehicle range by as much as 50% over that of a conventional stiff hull, even without taking into account the decreased volume and weight capacity of a vehicle with a heavier thick-walled cylindrical hull.

D. Electrical Design

Processor Board: The primary requirements for the Seaglider electrical design are low power, small size, and versatility to allow integration of current and future sensors. The low-power requirement necessitated a microcontroller capable of a submilliampere sleep mode and a large variety of power switches to turn on and off the various subsystems as required. The use of surface mount components was required to reduce

circuit board size. A large number of serial communication channels as well as analog and digital channels were required for sensor integration.

We chose the Onset Computer Corporation's TT8 controller as the main electrical component. This controller utilizes the versatile Motorola MC68332 microcontroller combined with a 12-b A/D converter and power conditioning circuitry on a small (~5 cm by 7.5 cm) printed circuit board. A unique connector system allows access to virtually all signals on the board within the small footprint. Main memory storage is accomplished with the Peripheral Issues CF8 Compact Flash memory expansion product which attaches to the TT8 through these connectors. A 48 megabyte Compact Flash disk is used for program and data storage. The combination of the TT8 and CF8 OEM products are then integrated to a custom designed main circuit board incorporating a wide variety of analog and digital interfaces, power control and conditioning circuits, and interface connectors.

Power Budget: The usefulness of the Seaglider relies heavily on power conservation. This is accomplished though the use of power control circuits and low-power circuitry as well as concurrent execution of software tasks. Two battery packs are used in the Seaglider design to maximize efficiency and isolate motor power from digital/analog power. The low (10 V) and high (24 V) voltage packs use 18 and 63 lithium thionyl chloride D-cell batteries, respectively. These packs are rated at 0 °C to carry 2161 and 7763 kJ of energy, respectively.

Energy use is highly dependent upon mission goals and environmental conditions. The depth, data sampling rate, and dive cycle period predominately determine the energy budget for a dive cycle.

Attitude Sensing Package: The Precision Navigation, Inc., model TCM2-80 attitude sensor package is used to measure vehicle pitch, roll, and magnetic heading. The TCM2-80 is rated to operate at pitch and roll angles as steep as 80° from horizontal while the maximum Seaglider pitch is about 45°. This attitude sensor uses a biaxial electrolytic gravity sensing inclinometer and a three-axis magnetometer to sense three-dimensional (3-D) attitude. We have examined heading, pitch, and roll accuracy for each TCM2-80 unit we have installed in a glider by monitoring outputs at 440 pitch/roll/heading orientations (−75° to 75° in pitch, −30° to 30° in roll, and every 45° in heading) on a compass calibration table located outdoors in a magnetically clean environment. Errors in TCM2-80 reported heading typically exceed 45° for mixed pitch-roll combinations of 45° or more.

Because the magnetometer outputs are available from the TCM2-80, heading can be computed by the user based on correcting pitch and roll. Pitch errors were observed to be heading-independent for a given roll (as should be the case), up to 5° or so in amplitude for a roll of 30° (smaller for smaller rolls), and could adequately be fit by the sum of a bias, a linear trend, and the first harmonic in pitch. The fits reduced pitch error to about a quarter degree. Using corrected pitch and the TCM2-80 magnetometer readings results in heading errors of only several degrees that vary smoothly as a function of heading. This error was further fit by a bias plus two harmonics of azimuth to reduce heading errors to less than 1°.

Navigation Receiver: Seaglider uses a Garmin 25HVS GPS receiver.

Data Telemetry: Seaglider uses a Sierra Wireless MP205 wireless modem for bidirectional data telemetry. The MP205 uses Circuit Switched Cellular (CSC) communications over the Advanced Mobile Phone Service (AMPS) cellular network and can transmit up to 3 W of power. Over this network, Seaglider uses the YMODEM file transfer protocol to transfer data and command files to a host computer on shore. Typical data throughput rates are around 450 bytes/s and about 26 J/kbyte energy rate. An overhead of about 40 s is required to establish a data connection at an energy cost of 180 J.

In order to operate offshore, a low-power satellite data telemetry system is necessary. Use of one or more of the existing and planned systems is anticipated.

Antennas: Seaglider mounts the GPS and wireless modem antennas at the end of its antenna mast. The antennas are waterproofed by potting both antennas into a mold along with the graphite tube. The mold is designed so that the antennas are in a vertical orientation when Seaglider is at the surface. Neoprene jacketed coaxial cable and impedance controlled coaxial subsea connectors are used for bringing the RF signals from the antennas into the Seaglider pressure housing. The GPS antenna is an active patch antenna from Micropulse, Model 1880ZW. The wireless modem antenna is a custom dipole tuned to the AMPS cellular network frequency band.

Scientific Sensors: The basic scientific instrumentation on Seaglider is a conductivity–temperature–depth (CTD) package. Output of the pressure sensor is used for vehicle control as well as labeling the depth at which temperature and electrical conductivity are measured. Addition of dissolved oxygen, fluorometer, and optical scattering packages is under development.

- Pressure

  Seaglider uses a Paine Corporation 211-75-710-05 1500PSIA pressure sensor. The sensor is temperature-compensated stain gauge type with an accuracy of ±0.25% full scale. The output of the sensor is digitized by a 24-b A/D converter.
- Temperature

  A Sea-Bird Electronics SBE 3 thermistor is mounted on the leading edge of a small fin that penetrates the top of the fairing between the wings. It is wired to electronics boards in the aft portion of the pressure hull.
- Conductivity

  A Sea-Bird Electronics SBE 4 conductivity cell is mounted on the top of the sensor fin in close proximity to the thermistor. To save power, the cell is flushed by flow past the glider instead of being pumped as is normally the case for profiling SBE conductivity sensors. This is possible because glider speed changes only slowly, providing a nearly steady flushing rate of the conductivity cell, just as provided conventionally by a pump.

E. Software Design

Dive Control Algorithm: The dive control algorithm is best described by considering a typical autonomous dive cycle sequence. At the sea surface, the glider moves the pitch mass fully forward to pitch the vehicle down, and pumps to obtain the target surface buoyancy necessary to raise the antenna the
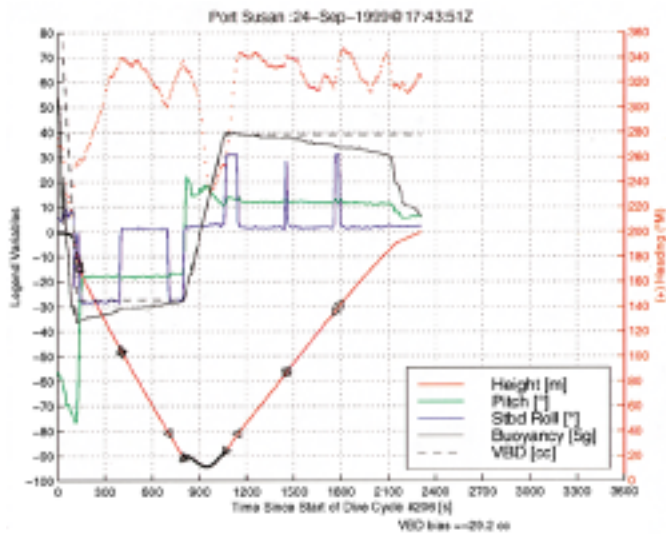
Fig. 5. Typical Dive Cycle Sequence. Leftward and rightward pointing triangles on the depth curve indicate the beginning and end of roll control actuation. Upward and downward pointing triangles similarly indicate pitch actuation. Solid black circles indicate changes in buoyancy control volume VBD. VBD has been corrected by the indicated bias in this plot.

desired amount above the sea surface. The GPS receiver is then powered and the glider waits to receive a fix of acceptable quality. Having done so, the glider initiates a (cellular telephone) call to the data logging and control computer located on a vessel or ashore. Once connection is established, the glider sends any data files that have not previously been sent successfully. Next, it gets the command file containing dive cycle parameters from the data logging/control computer. Parameter values in this file override those previously stored in the glider. The GPS position from before the call is sent and the data telemetry connection is broken. The glider then obtains a second GPS fix and uses it to update the estimated position calculated by the navigation control algorithm (see below).

A target vertical speed is chosen through the combination of the target depth and the time to complete a dive cycle. The glider tries to achieve and maintain a uniform vertical speed by controlling its buoyancy at a set pitch. Pitch and desired buoyancy are chosen at the start of the dive to attain the desired glide slope angle and descent rate. Once the desired glide slope, heading, and buoyancy for the dive is calculated, the external bladder starts bleeding to the desired VBD volume (expressed relative to neutral buoyancy at the target dive depth and controlled to about 1 cc accuracy). This is when data collection at the specified sampling rate begins.

A typical dive cycle sequence is shown in Fig. 5. The glider begins to leave the sea surface when buoyancy becomes negative. As the antenna mast sinks below the surface, the glider attains its most extreme downward pitch, about $-75°$. Once bleeding is finished, triggered by VBD volume achieving its target value, pitch is adjusted to the level desired to attain the desired glide slope for the dive. By diving steeply from the sea surface, Seaglider builds momentum used to quickly achieve unaccelerated flight when pitch is adjusted to the desired value for the rest of the dive. In the example in Fig. 5, this transition takes place about 120 s after the start of bleeding at about

15-m depth (the transition occurs substantially shallower in less strongly stratified waters). Pitch control sensitivity is $1–2°$/mm of pitch mass movement.

The vehicle then rolls by about $30°$ to adjust its heading. Roll is to starboard to turn the glider to the left on descent, and the opposite for ascent. The asymmetry is because wing lift has a lateral component in the direction of roll that is applied aft of the center of buoyancy, causing the vehicle to turn in the opposite sense of its roll when diving. The opposite roll-turning sense relationship holds on ascent, since wing lift is downward in a climb. Typical turn rates, as can be seen in the dive cycle sequence, are $0.2–0.6°$/s, giving turn radii of a few tens of m at typical horizontal speeds of 0.20–0.25 m/s. In the dive in Fig. 5, the desired heading is achieved at about 50-m depth. Once heading is within a dead-band of that desired, the glider exits its active control mode and puts the microprocessor into low power sleep mode. It awakens from this mode briefly at the data sampling interval to make measurements of pressure, temperature, and conductivity.

At specified intervals (5 min in the case shown), the glider reenters the active guidance mode to check its descent rate and heading. It bleeds or rolls as necessary as it continues to dive. A roll maneuver made to correct heading was actuated about 700 s into the dive sequence shown in Fig. 5, since the vehicle had gradually turned $40°$ to the left in the previous 5-min interval.

When Seaglider detects a depth greater than the target depth, it pitches up and pumps to the opposite of the (uncorrected for bias) negative VBD volume value used for the dive. In the example in Fig. 5, the glider pitch was changed to opposite the dive pitch at the start of pumping. This caused the glider to rise initially, but then continue to descend until buoyancy changed sign. This has the effect of driving the glider slowly backward, an unstable configuration that causes it to change heading sharply. In later deployments, the glider pitches up only partially until VBD volume becomes neutral before pitching up to its desired ascent value. At the end of pumping, the glider again corrects its heading by rolling. Because of density stratification, the glider typically is most negatively buoyant shortly after a dive starts and is least negatively buoyant at the target depth. Conversely, it is most positively buoyant at the end of pumping at depth and least positively buoyant as it enters less dense surface waters.

Close to the sea surface the glider crosses another user-specified depth threshold, typically a few m, after which it collects a fixed number more samples before pitching down and pumping to raise the antenna above the sea surface. This completes a dive cycle.

Data Structure: Separate files contain routinely acquired measurements (the data files) and parameter settings and control history for each dive cycle (the log files). Each record in data files includes depth, temperature, conductivity, heading, pitch, and roll samples and pitch control, roll control, and VBD volume. These files are compressed by storing blocks of nine records of differences following a record with full resolution. In order to conserve power, data files are broken into several smaller ones to avoid retransmitting large files if errors are detected.

Navigational Control: Seaglider approaches and remains near its designated target position using a Kalman filter routine

to assimilate the differences between the sequence of actual surface positions and those positions projected by dead reckoning during dive cycles. In regions where tidal currents are comparable in speed to glider horizontal speeds, the Kalman prediction scheme allows Seaglider to expend power efficiently. The Kalman filter implemented by Seagliders models water displacement as the sum of mean, diurnal, and semidiurnal components. The routine chooses glider speed and heading (the control vector) for a dive cycle on the basis of projected currents during the cycle. The GPS position at the start of each dive cycle is used to update the estimated glider position. Seaglider chooses the control vector that will make most progress toward reaching the target subject to the constraints of minimum and maximum speed limits imposed by specifying maximum dive angle magnitude and maximum buoyancy to be used. In the case that currents are too strong for the glider to reach a target, it chooses a course which minimizes the increase in target range.

III. FIELD PERFORMANCE

A. Summary of Field Tests

Seagliders have been deployed on over a dozen occasions to date at various locations in Puget Sound, WA, and in Monterey Bay, CA. Initial tests involved making single dive cycles after which the first Seaglider was recovered and returned to the work vessel for data transfer, reprogramming, and any necessary repairs. Incorporation of successful data telemetry capability enabled autonomous operation. Most recently we have operated two gliders simultaneously in Possession Sound, a 1.5–2-km-wide, 180–200-m-deep section of Puget Sound.

B. Hydrodynamic Performance

The first use of Seaglider in autonomous mode was to execute dive cycles to target locations at various ranges to assess hydrodynamic performance. We chose a portion of Port Susan, part of Puget Sound, WA, for these dives for its depth (∼100 m), weak tidal flow (∼0.05–0.1 m/s), and logistic ease. The work vessel was anchored from both bow and stern to minimize its movement and an acoustic Doppler current profiler (ADCP) was mounted from its rail to monitor currents during glider dives. The glider was tracked using a synchronous tracking range using four hydrophones separated by O(10 m) horizontally with better than 1-m accuracy. Using estimates of vertical speed inferred from the vehicle pressure record, horizontal speed components calculated as the difference between acoustically tracked speed and current relative to the vessel, vehicle pitch angle, and buoyancy inferred from glider CTD measurements, regressions against the hydrodynamic model were performed.

The results of a regression against 14 4–min average intervals chosen from among 9 different dive cycles with glide slopes ranging from 3 : 2 to 1 : 4 gave estimates of the hydrodynamic parameters a, b, and c that were similar to those found from wind tunnel regressions. Profile drag was about 30% higher than that inferred from the wind tunnel measurements. A plausible explanation is that the increased drag found in the field data
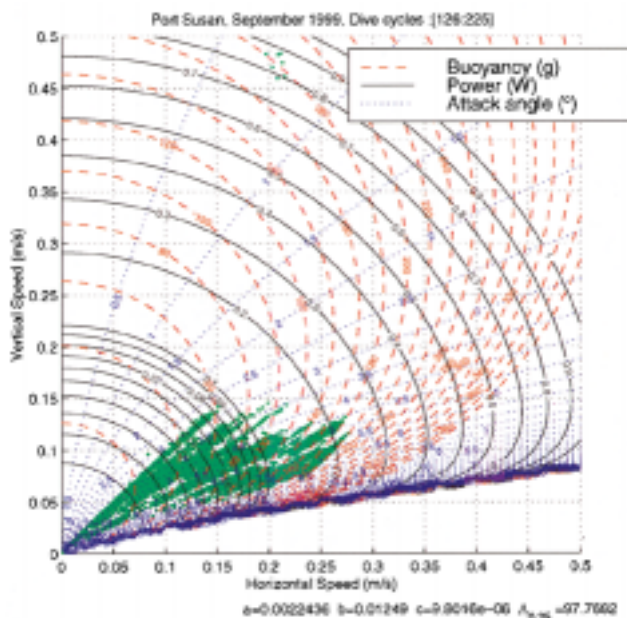

Fig. 6. Performance of Seaglider based on vertical velocity implied by hydrostatic pressure changes. Buoyancy expressed as a gram-force is contoured in dashed red, power consumption in watts in solid black, and attack angle in degrees in dotted blue. The green symbols mark data points labeled with observed buoyancy. The standard deviations of the misfit in drag force, the quantity minimized, and that of buoyancy are indicated by σ_{drag} and σ_{bouy}. The buoyancy bias, lift and drag parameters, and performance factor for 0.25 m/s flight are also indicated. The contoured region is where unaccelerated flight is possible. The implied stall glide slope varies from 1 : 4 to 1 : 6, depending on speed.

is due to the conductivity sensor mount and the antenna mast assembly, absent from the wind tunnel study.

Estimates of the hydrodynamic parameters a, b, and c found from minimizing the difference between observed and model vertical velocity from a hundred dive cycles or more in Port Susan are very similar. Results for such a regression are shown in Fig. 6. In this case, 15 259 estimates of vertical velocity, buoyancy, and pitch taken 8 s apart from 100 successive dive cycles at a variety of glide slopes were used in the regression. The vertical/horizontal speed pairs implied by the measured pitch and buoyancy values are plotted in Fig. 6 to indicate the distribution of speeds and glide slopes used in the regressions. As in the regressions using the tracked data, these regressions minimizing the implied vertical water velocity also give a drag parameter b somewhat greater than that found in the wind tunnel study and similar performance factors.

Less than 7% of the observed vertical speeds differ from the model by more than 2 cm/s. The standard deviation of the difference between observed and model vertical velocity, 1.26 cm/s, is a plausible value for natural vertical motion of water in Puget Sound due to internal waves and turbulence. The difference between observed and model glider vertical motion shows promise as a measure of sufficiently strong vertical motion in the ocean. An example is given below.

C. Field Measurements

The first multiday mission a Seaglider was an eight-day transect through Port Susan, one of the fjords making up Puget Sound. All GPS fixes taken during this 225 cycle mission are
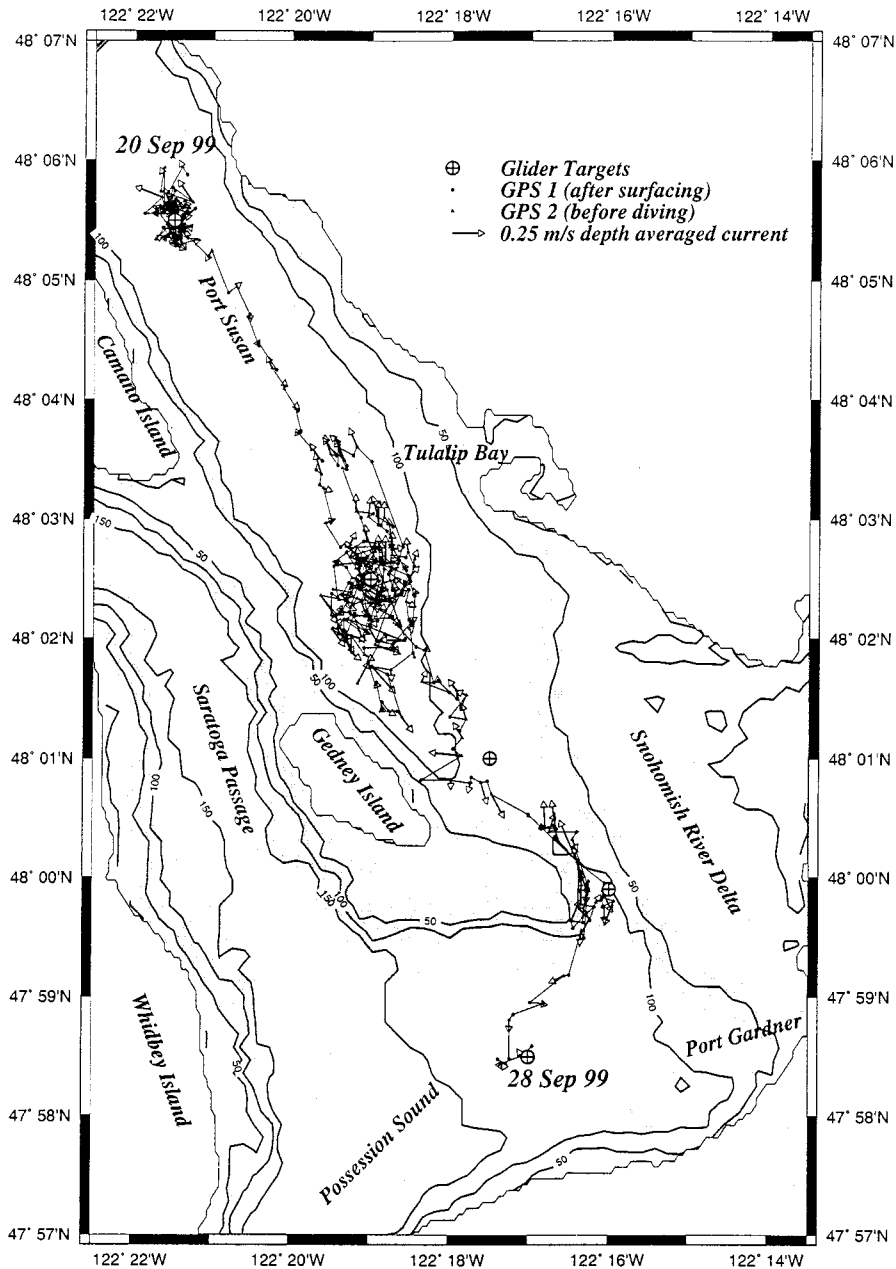
Fig. 7.   Seaglider track from Port Susan to Possession Sound, September 1999. Pairs of GPS fixes are plotted between dive cycles. Arrows indicate depth averaged current inferred from the difference between actual and dead-reckoned displacements. Depth contours are in meters.

plotted in Fig. 7. The vehicle was launched about 800 m from its first intended target, programmed to make hourly dives to a depth of 90 m. After two days, during which it stayed within about 400 m of its target, it was commanded by a file sent from a computer at UW to move to a second target about 3 km north of Gedney Island. At the new target, Seaglider encountered stronger tidal currents than at its previous location. During the process of adjustment by the Kalman filter navigation control scheme, a storm with 20-m/s surface winds crossed the region. GPS fixes were not received for hours, presumably due to enhanced sea state, during which the glider moved over 2 km north of its target. Once fixes were again received, the glider continued to assimilate tidal currents, but having been fooled by the wind burst into inferring a strong diurnal current, it to attempted to compensate for anticipated northward drift one day

later by transiting 2 km south of the target, within 800 m of Gedney Island. The glider tended to orbit the target in a clockwise sense, spiraling gently toward it. This was due to a tendency for the glider to travel about 15° to the left of the heading chosen by the Kalman filter. This difference was due to a dead reckoning scheme that corrected heading without correcting for accumulated lateral displacement from the desired track.

After 4.5 days near the second target, the glider was sent in turn to three more targets that took it from Port Susan to Possession Sound through a passage 500 m wide at the dive cycle depth. Once through the passage the first time, the glider was drawn back through it on the opposite phase of the tide, unable to overcome the current with the maximum 166 g of buoyancy magnitude it was allowed to develop. Seaglider successfully exited the narrow passage and was recovered from an inflatable boat using
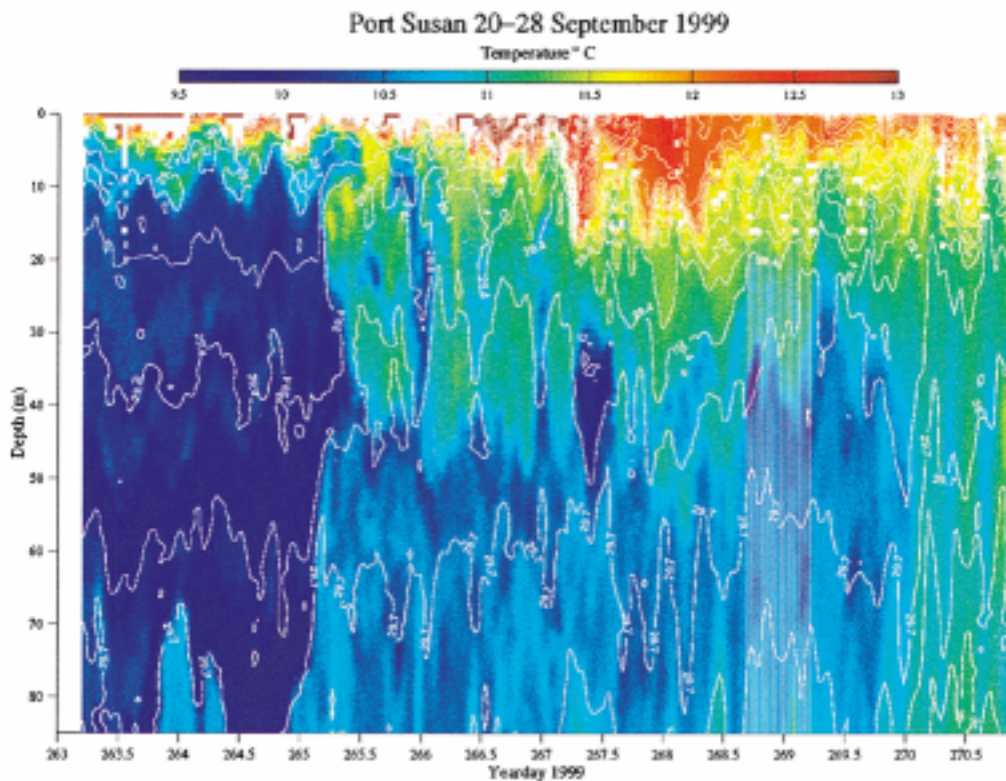
Fig. 8. Salinity and temperature mapped on a 1-m, 1-h depth–time grid from the September 1999 Port Susan glider deployment. Salinity is contoured at 0.15-psu intervals.

a only a GPS receiver and instructions called to it by cellular telephone from UW to locate it visually. The mission was terminated after 225 dive cycles because of concerns about the remaining capacity in the previously used battery packs employed.

A depth–time section of temperature and salinity mapped from the glider mission is given in Fig. 8. The glider sampled temperature and salinity every 8 s while diving and climbing at roughly 0.5 m/s, allowing depth resolution of 0.5 m or so (the map resolution is 1 m). Stratification in Port Susan is dominated by salinity, as can be seen from the 1–2 psu contrast from the top few meters to an 85-m depth. Temperature acts largely as a tracer in the estuarine flow, hence temperature inversions are commonly observed. Prominent oscillations at semidiurnal tidal periods are evident in both fields, showing vertical excursions of 10 m or more. There is also a trend evident from cooler fresher water sampled in the first two days to warmer saltier water observed at depth in the rest of the record. Isopycnals rise $\sim$25 m from the beginning to the end of the section, describing the salt wedge structure of an estuary (warm salty water of oceanic origin is drawn in at depth by mixing of cool fresh water of riverine origin). Also evident is the deeper, more diffuse pycnocline produced by mixing associated with the wind event that occurred on year day 267.

Besides temperature and salinity profiles, Seaglider data can be used to estimate current averaged over the depth of dive cycles from the difference between dead-reckoned displacements and those found from GPS fixes at the surface. Since vehicle buoyancy can be estimated from the difference between water density and vehicle density (since vehicle volume is measured
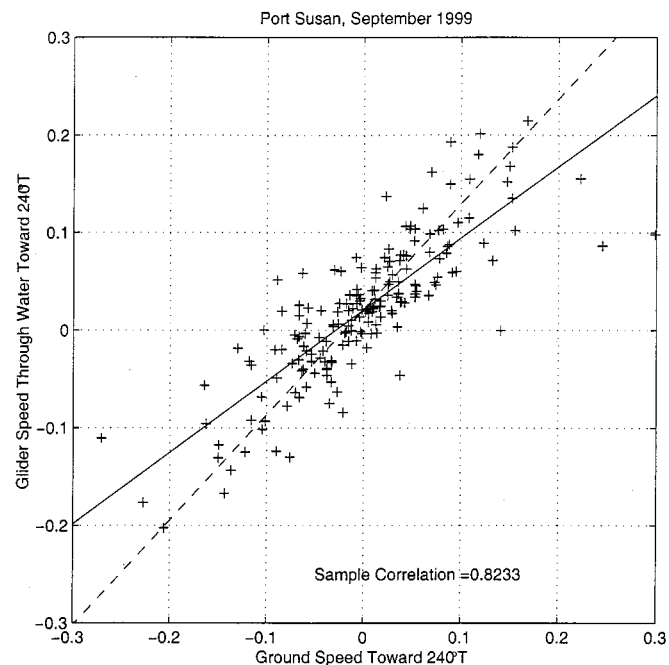

Fig. 9. Scatter plot of the cross-channel component of glider speed through the water over a $\sim$1-h dive cycle with over ground speed derived from GPS fixes. Lines indicate linear regressions of each variable upon the other.

to an accuracy of 1 cc or better) and vehicle pitch is measured to an accuracy of better than 0.5°, glider speed through the water can be estimated from the hydrodynamic model. Uncertainty in buoyancy of $\sim$5 g and in pitch of $\sim$1° implies an uncertainty

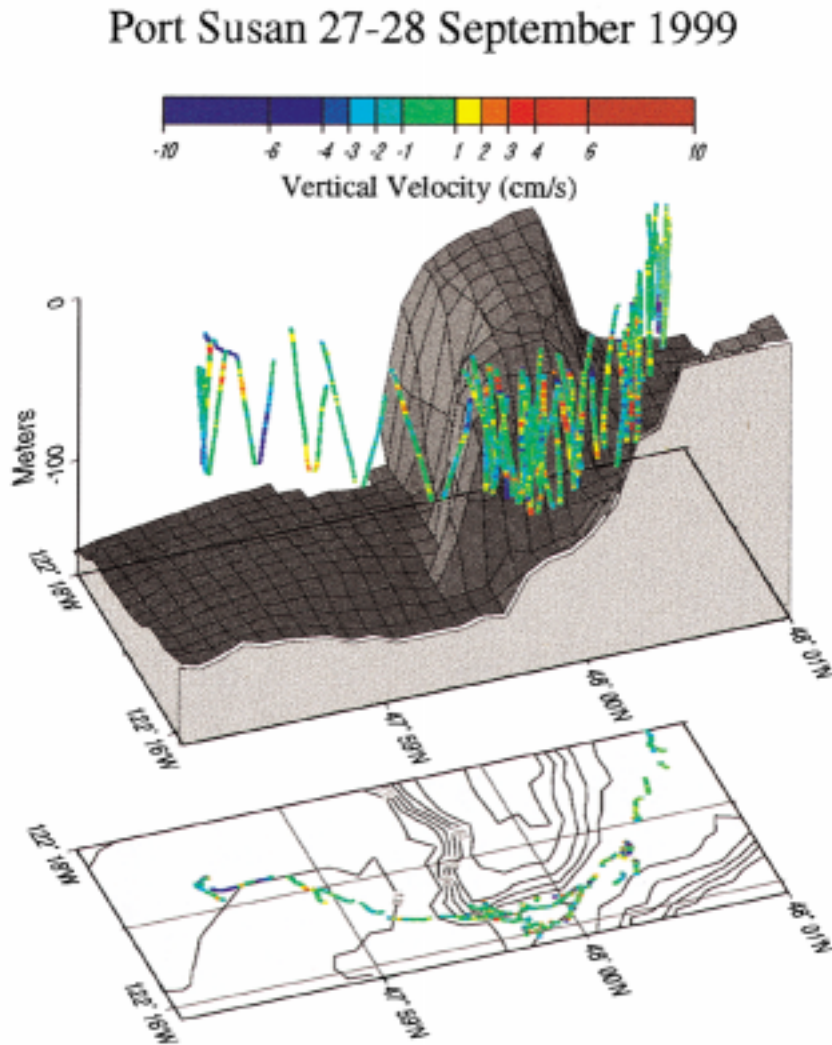## Port Susan 27–28 September 1999

Fig. 10. Vertical velocity inferred from the difference between observed and model glider vertical motion rates in the narrow passage SE of Gedney Island connecting Port Susan (shallower, to the right as depicted) to Possession Sound (deeper, to the left).

in horizontal speed of ∼1–1.5 cm/s. This uncertainty is smaller than that from 100 m error in GPS fixes taken an hour apart. Uncertainty of ∼1 cm/s in speed components is comparable to that for moored current meters. Depth-averaged (0–90 m) current estimates are shown along the glider track in Fig. 7. While we have no independent current estimates with which to compare the glider-derived estimates, current components in the cross-channel direction in Port Susan can be expected to be weak so this component of glider speed through the water and GPS-derived speed over the ground should be highly correlated. A scatter plot and regressions (Fig. 9) show these components to explain over 82% of each other's variance and to be linearly related to one another by a gain indistinguishable from unity. The standard deviation of the unexplained signal is 0.03 m/s or less. The unexplained variance could easily be attributed to noise in successive GPS fix positions plus any actual cross-channel flows. The high correlation and unit gain suggest that glider depth-averaged current estimates are credible and have a noise level that can be reduced by averaging both longer dive cycles and many of them.

Knowledge of vehicle buoyancy, pitch, and hydrodynamics also allows estimates of vertical velocity. As mentioned above, the standard deviation of the difference between observed and model vertical velocity is 0.015 m/s or smaller in Port Susan. In most of the Port Susan dive cycles, the implied vertical water speed is smaller than 1 cm/s and varies with scales comparable to the 90-m dive cycle depth. The exception is in the narrow passage between Port Susan and Possession Sound where depth-averaged currents as high as 0.4 m/s were inferred. Unlike dive cycles in quieter regions where glider depth changes almost linearly with time for the most part, vehicle depth changes were somewhat irregular in the narrow passage, even opposite in sense to the applied buoyancy for tens of seconds. These irregularities are presumed due to vertical water speeds of 0.05 m/s or more over depth ranges of 10–40 m (Fig. 10). Vertical velocities of this magnitude are common in tidal flows over topographic features. In this case, sloshing of the tide through a passage connecting basins 50 m different in depth is the likely source of internal waves and turbulence that produce prominent vertical velocity signals.

IV. DISCUSSION

Seagliders offer the prospect of collecting oceanographic measurements at deliberately chosen remote locations and reporting them promptly at a comparatively low cost. They can be used to study phenomena on a wide variety of space and time scales, from one to thousands of kilometers and hours to decades. While long surveys made with solitary gliders would be aliased by temporal variability and time series at single locations would suffer similarly from spatial variations, the use of multiple vehicles in transit, "virtually moored," or a mixture of these modes offers promise in resolving oceanic variability. While gliders move slowly compared to the swiftest oceanic currents, as long as depth-averaged flows are sufficiently weak, gliders can make headway against ambient flows. Even when this is not the case, as with the prominent western boundary currents, gliders could be commanded to deliberately be swept downstream in transiting them and to return upstream in regions where the flow is weaker. Repeated transects across boundary currents would be possible by completing circuits that take advantage of the flow structure being studied.

One of the key features of glider technology is that measurement strategies can be altered on the basis of what is measured. Data-adaptive sampling can be manually determined by operators or can be automatic, as is the case for Seagliders in attempting to compensate for currents as they sample.

Seagliders successfully use a low-drag shape to enhance the range and duration of deployments. Their performance demonstrates drag less than half that of conventional torpedo-shaped vehicles with the same volume [11]. For equivalent lift, a low-drag buoyancy-driven vehicle can travel more than twice as far than one with a conventional shape for the same energy cost.

A novel feature of Seaglider is its ability to profile temperature and salinity and concurrently estimate depth-averaged flow. Consider a pair of Seagliders at "virtually moored" at distinct locations from which temporally averaged density profiles can be calculated. In principal, the implied vertical shear may be combined with the temporally averaged depth-average current over the dive cycle depth to estimate absolute geostrophic current (neglecting frictional flows such as Ekman transport). The determination of geostrophic reference levels is the fundamental difficulty that has hampered attempts to describe ocean circulation from hydrography.

Other sensors may be added to gliders without compromising their performance severely as long as they are suitably small, use little power, and do not disrupt glider flight. Since the average overall power consumption of Seagliders is on the order of 0.5 W, sensing systems that use small amounts of power only intermittently are most suitable. Size and weight as well as hydrodynamic drag are important to vehicle performance through ballast and trim considerations. We are in the process of adding a dissolved oxygen sensor and two bio-optical sensors, a fluorometer, and a backscatter sensor.

ACKNOWLEDGMENT

REFERENCES

[1] R. E. Davis, D. C. Webb, L. A. Regier, and J. Dufour, "The autonomous Lagrangian circulation explorer (ALACE)," *J. Atmos. Oceanic Technol.*, vol. 9, pp. 264–285, 1992.

[2] R. E. Davis, "Preliminary results from directly measuring middepth circulation in the tropical and South Pacific," *J. Geophys. Res.*, vol. 103, pp. 24 619–24 639, 1998.

[3] S. Wilson, "Launching the Argo armada," *Oceanus*, vol. 42, pp. 17–19, 2000.

[4] H. Stommel, "The Slocum Mission," *Oceanography*, vol. 2, no. 1, pp. 22–25, 1989.

[5] K. Wyrtki and B. Kilonsky, "Mean water and current structure during the Hawaii-to-Tahiti shuttle experiment," *J. Phys. Oceanogr.*, vol. 14, pp. 242–254, 1984.

[6] M. J. McPhaden, "Genesis and evolution of the 1997–98 El Nino," *Science*, vol. 283, pp. 950–954, 1999.

[7] H. M. Stommel, "Discussions on the relationships between meteorology and oceanography," *J. Mar. Res.*, vol. 14, pp. 504–510, 1955.

[8] J. S. Parsons *et al.*, "Shaping of axisymmetric bodies for minimum drag in incompressible flow," *J. Hydronautics*, vol. 8, no. 3, 1974.

[9] R. M. Hubbard, "Hydrodynamics technology for an Advanced Expendable Mobile Target (AEMT)," Applied Physics Laboratory—Univ. of Washington, Rep. no. 8013, 1980.

[10] S. A. Jenkins and J. Wasyl, "Optimization of glides for constant wind fields and course headings," *J. Aircraft*, vol. 27, pp. 632–638, 1990.

[11] R. M. Hubbard and H. R. Widditsch, "The relative cost effectiveness of low drag versus conventional target vehicles," Applied Physics Laboratory—Univ. of Washington, Rep. no. 7910, p. 25, 1979.

Charles C. Eriksen received the A.B. degree in engineering and applied physics from Harvard University, Cambridge, MA, in 1972 and the Ph.D. degree in oceanography from the Massachusetts Institute of Technology (MIT)—Woods Hole Oceanographic Institution (WHOI) Joint Program in Oceanography, Woods Hole, MA, in 1977.

He is a Professor in the School of Oceanography, University of Washington, Seattle. After a post-doctoral appointment at WHOI, he joined the MIT faculty in 1977 and moved to the University of Washington faculty in 1986. His interests are in observing and understanding physical processes in the ocean, among them upper ocean, tropical, boundary current, and estuarine dynamics. Until the development of Seagliders, most of his observational work was carried out using deep sea moorings.

T. James Osse received the B.S. and M.S. degree in mechanical engineering from the University of Washington, Seattle, in 1979 and 1981, respectively.

He is a Senior Ocean Engineer in the Applied Physics Laboratory at the University of Washington. He has spent 17 years in the design and field operation of various ocean engineering systems, specializing in small autonomous underwater vehicles and drifting Lagrangian instruments. He was program manager and lead engineer for the Autonomous Line Deployment Vehicle, an 8-kg submersible used in three Arctic field operations with over 75 successful missions. He designed two generations of the Mixed Layer Float as well as the Deep Lagrangian Float, both drifting, isopycnal oceanographic floats. More recently he was the project manager and lead engineer developing the Seaglider. He is a university certified diver with 14 years experience. He joined the Applied Physics Laboratory of the University of Washington in 1982 and is presently on a leave of absence.

Russell D. Light received the B.S. degree in electrical engineering from the University of Washington, Seattle, in 1982.

He is Head of the Ocean Engineering Department at the Applied Physics Laboratory (APL), University of Washington, and has worked at APL since 1982. He worked for five years on Naval acoustic targets for torpedo testing followed up by a number of projects in ocean instrumentation including solid-state data recorders, underwater tracking ranges, a mine training device for Navy EOD divers, and benthic sonars. During the 1990s, he was the lead electrical and systems engineer for several autonomous undersea vehicles that were used for scientific missions under the Arctic ice pack. Most recently he has been the project manager and lead electrical engineer developing the Seaglider.

Timothy Wen, photograph and biography not available at the time of publication.

Thomas W. Lehman, photograph and biography not available at the time of publication.

Peter L. Sabin, photograph and biography not available at the time of publication.

John W. Ballard, photograph and biography not available at the time of publication.

Andrew M. Chiodi, photograph and biography not available at the time of publication.